processes

MDPI

Article

Rubber Tiles Made from Secondary Raw Materials with Immobilized Titanium Dioxide as Passive Air Protection

Paula Benjak [1,*], Lucija Radetić [1], Marija Tomaš [1], Ivan Brnardić [2], Benjamin Radetić [1], Vedrana Špada [3] and Ivana Grčić [1]

[1] Faculty of Geotechnical Engineering, University of Zagreb, Hallerova Aleja 7, HR-42000 Varazdin, Croatia
[2] Faculty of Metallurgy, University of Zagreb, Aleja Narodnih Heroja 3, HR-44000 Sisak, Croatia
[3] METRIS Research Centre, Istrian University of Applied Sciences, Riva 6, HR-52100 Pula, Croatia
* Correspondence: benjak.paula@gmail.com

Abstract: The immobilization of titanium dioxide, particularly commercial TiO_2 P25, on the surface of recycled rubber tiles presents a solution for achieving passive air protection. A completely new purpose for tiles was obtained by addressing air pollution and related health issues. Modified rubber tiles were prepared using a sol–gel method with three different proportions of TiO_2 (2, 4, and 10 g) in the solution. The nature of TiO_2 nanoparticles and their respective binding on the tile surface was determined using scanning electron microscopy (SEM) equipped with electron dispersion X-ray spectrometry (EDS) and Fourier-transform infrared (FTIR) spectroscopy. The SEM-EDS results showed that the most successful immobilization was achieved with the lowest amount of TiO_2 in the sol–gel solution. The FTIR results confirmed a band at 950 cm^{-1} that was attributed to the Ti-O-Si bond. The stability and environmental impact of the treated rubber substrates were investigated by a leaching test. Photocatalytic oxidation was confirmed by the oxidation of NH_3 to N_2. Based on the results obtained, rubber substrates with an addition of 2 g of TiO_2 have demonstrated prospects for further tests of the photocatalytic degradation of airborne pollutants.

Keywords: advanced oxidation processes; heterogeneous photocatalysis; titanium dioxide; air treatment; recycled rubber

Citation: Benjak, P.; Radetić, L.; Tomaš, M.; Brnardić, I.; Radetić, B.; Špada, V.; Grčić, I. Rubber Tiles Made from Secondary Raw Materials with Immobilized Titanium Dioxide as Passive Air Protection. *Processes* **2023**, *11*, 125. https://doi.org/10.3390/pr11010125

Academic Editors: Zhenghua Zhang and Blaž Likozar

Received: 9 November 2022
Revised: 23 December 2022
Accepted: 26 December 2022
Published: 1 January 2023

1. Introduction

An environmentally friendly and low-cost rubber recycling method is currently one of the biggest environmental challenges of the 21st century [1]. The management of waste tires in Croatia has been progressively improved. The first company that recycled the rubber of used car tires was founded in 2005. The main goal was to reduce the harmful impact on the environment while reusing the valuable properties of rubber; in this case, the end goal was the production of recycled rubber tiles. The primary purpose of recycled rubber tiles is to provide protection from injuries on children's playgrounds; they are also used for many other purposes [2,3]. Rehabilitation centers in closed and open spaces are much safer if the surface is covered with rubber tiles as opposed to, for example, ceramic tiles. Today, noise is defined as one of the factors that pollute the working and living environment, so it is important to note that rubber tiles reduce the noise level by up to 32 dB, which is important for places where sports fields and fields are located [2,4]. Rubber elements are used as sound insulators, anti-vibration mats, sealants of various types, roofing panels, buffers in harbors for the berthing of vessels, floating docks, and as various non-slip mats, etc. [2,5]. It is estimated that the construction industry will become the largest consumer of rubber granules and tiles due to the need to create sound barriers, structural stiffeners, and accessories for foundations, etc. [2,6]. The tiles are made of granules of different sizes (the technological process is explained in more detail in the methodology). This contributes to the roughness of the tiles and is responsible for anti-slip performance. Unfavorable weather conditions very often prevent the use of playgrounds or

fields due to water retention, but rubber surfaces—due to their waterproofness—enable use regardless of the weather. "Tires are primarily vulcanized rubber, rubberized fabric, steel or fabric belts, and steel-wire-reinforced rubber beads. The most commonly used tire rubber is styrene-butadiene copolymer (SBR) and consists of about 75% butadiene and 25% styrene by weight [7]". Other elastomers akin to natural rubber are also used in differing amounts in tire compounds. The most-used fillers are carbon black, extender oil, and sulfur [7].

Currently, the basic methods of waste-rubber recycling are shredding and grinding. To ensure the effective recycling of waste rubber, separating all unnecessary parts from the rubber (such as iron castings and textiles) is necessary [1]. Old, exported tires give granules of various sizes with modern technology. In this paper, a special emphasis is placed on the recycled rubber tiles that line children's playgrounds, sports and recreational facilities, and rehabilitation centers. Our main purpose is to extend the functionality of rubber tiles from an environmental point of view. Recently, people's awareness of environmental pollution and its negative consequences has been increasingly awakened. Although industrial development affects air quality, it also encourages the advancement of technology and the interest of scientists, leading to its inevitability.

The application of heterogeneous photocatalysis in air purification has been developed over the last decades. The gas-phase photocatalysis was developed in work based on the photodecomposition of nitric oxide [8]. Given that a wide range of air pollutants can be partially or completely degraded with TiO_2-assisted UV irradiation, over the years several studies have suggested using the solid–gas photocatalysis for environmental applications [9–13]. Heterogeneous photocatalysis became popular after Fujishima and Honda discovered the UV-driven, photoelectrochemical water-splitting reaction with a TiO_2-based photoanode in 1972 [14]. This is a process in which solar radiation, in synergy with a photocatalyst and in the presence of water molecules, creates a chain of redox reactions on the surface of the photocatalyst, resulting in inert products such as carbon dioxide, water, and other non-toxic species, depending on the structure of pollutant (as is shown in the graphical abstract). Under the source of UV radiation, the electrons in the photocatalyst's valence band are promoted to its conduction band, thus leaving an empty space—or so-called hole (h+)—with a lack of negative charge (e–) in the valence band. These holes are crucial for the initiation of redox processes which lead to pollutant degradation because they produce hydroxyl radicals (-OH) in the presence of humidity. These radicals react non-selectively with pollutants, oxidizing them to harmless molecules [15].

The advantage of photocatalysis is that it is an inexpensive, sustainable, and eco-friendly technology that results in a complete or partial decomposition of pollutants. The synergistic action of solar radiation and photocatalysts triggers redox reactions on photocatalysts surfaces which successfully remove sulphur dioxide, ammonia, unpleasant odors, volatile organic compounds, and nitrogen oxides, etc. [16]. For example, one of the most-researched photocatalysts, titanium dioxide (TiO_2) irradiated with UV light, can decompose many organic compounds into water, carbon dioxide, and mineral acids or their salts [17]. TiO_2 is widely used as an air purifier in various forms of coatings. For instance, Murugan et al. proved the performance of the self-cleaning coatings on building materials such as ceramic glazed tiles and glass windows. Nano TiO_2 films were generated in the form of a spray, dip, or as a flow coating method. The TiO_2 photocatalytic layer acts as a surface modification of such building materials, thus keeping the building exterior clean by utilizing solar energy [18]. Wang et al. also used nano TiO_2 powders such as Degussa P25 for concrete coatings to enhance the photocatalytic activity. Furthermore, nano-TiO_2-based coatings have been studied to improve the air purification and self-cleaning properties of cement-based materials [19], since those materials in buildings are directly and continuously exposed to various atmospheric pollutants and microorganisms under different weather conditions. Furthermore, new, industrially produced photocatalytic tiles by Bianchi et al. were made using a commercial micro-TiO_2. In addition to good photocatalytic performance, these tiles also meet standard requirements regarding porosity, durability, hardness, and vitrified surface. Photocatalytic degradation tests were performed

using NO_x and methylene blue as modeled polls for confirming good performance in both phases, gas and liquid [20]. Grčić et al. showed the application of solar photocatalysis for air purification by applying an alternative, best-available-technique TiO_2 photocatalysis. Toxic substances normally related to agriculture emissions, such as ammonia and methane, were included. Photocatalytic oxidation confirmed the continuous oxidation of NH_3 and CH_4 to CO and CO_2, and N_2, respectively [15]. TiO_2 as a photocatalyst was also used in synthesized compounds to improve certain properties, such as $TiO_2/ZnTiO_3$ [21], WO_3/TiO_2 [22], N–V co-doped TiO_2 [23], and TiO_2/zeolite composite [24], etc. The idea to test the application of rubber tiles with a photocatalytic layer for passive air protection was developed with these above-mentioned applications in mind.

The use of secondary raw materials—in this case recycled tires, which are used to produce rubber tiles—already represents ecological progress for the purpose of environmental protection. Additionally, this work presents a solution for achieving the passive protection of air and human health by immobilizing TiO_2 on the surface of recycled rubber tiles, based on which we will achieve a completely new purpose for substrates. The combination of tiles made from secondary raw materials and the achievement of photocatalytic decomposition of harmful compounds in the air gives additional value to this product in the context of a circular economy and environmental protection. Methods and results are provided in the following sections.

2. Materials and Methods

2.1. Rubber Tile Manufacturing

Rubber tiles made from recycled rubber were obtained from a recycling company, Gumiimpex-GRP, Ltd., Varaždin, Croatia. The process of manufacturing recycled rubber tiles begins with the collection of waste tires, followed by the acceptance, storage, sorting, mechanical processing (cutting and shredding), painting (depending on preference, occasion, and purpose), and finally production of the rubber tiles. The collected waste tires are divided and separated into passenger, cargo (dumper and truck), semi-truck, tractor, and forklift categories. Parts that are not of rubber origin, such as rims or tubes, must be separated. Mechanical processing cannot begin until the steel parts are separated. Cargo tires contain steel "bulks", so the first step is to remove them. Separated rims and steel "bulks" represent secondary raw materials and are sold further on the market. After all the tires have been sorted and all the steel parts have been removed from them, the first part of the mechanical processing follows: cutting. Tires of larger dimensions, such as dumper tires, truck tires, etc., are cut, while those of smaller dimensions enter the process whole. The cutting of large tires is performed in a machine with large knives. The tires are cut so that they can enter the second part of the mechanical processing: shredding, which is performed using a "shredder". The loader transfers cut tires into the shredder, which shreds the tires to a size of 100 × 250 mm. After the tires have been shredded for the first time, they pass through a vibrating screen and arrive on a conveyor belt which takes them to the raw material warehouse, where further shredding begins. After the tire is shredded to a size of 100 × 250 mm, it enters the first granulator via conveyor belt, where it is shredded to a maximum size of 30 mm. During this shredding, approximately 80% of the steel wire and textiles are released. The wire is transferred to the steel purification line, and the textile is separated pneumatically (i.e., by suction). Following this, the shredded rubber, which reaches a maximum size of 30 mm, enters the second granulator, where it is shredded to a maximum size of 12–14 mm. As with the previous granulator, steel wires and textiles are additionally separated. The third granulator shreds the rubber to a maximum size of 8–10 mm, and the fourth and fifth granulators shred the rubber to a maximum size of 3.0–3.5 mm. The last stage of purification from steel wires and textiles is carried out inside a rotating system for the separation of granules in which the iron and textiles are finally separated from the granules with additional suction and smaller magnets. After the sliced tires have undergone shredding through five granulators, the final raw material is obtained and is ready for further processing and the production of

recycled rubber substrates. The final product is a granulate in size ranges of 0.0–0.5 mm, 0.5–2.0 mm, and 2.0–3.5 mm (Figure 1).

(**a**) (**b**) (**c**)

Figure 1. Granules of sizes (**a**) 0.0–0.5 mm, (**b**) 0.5–2.0 mm, and (**c**) 2.0–3.5 mm.

After mechanical processing, the obtained rubber granulate is ready to produce tiles. The line to produce recycled rubber tiles consists of (1) an industrial mixer, (2) a press, (3) a material transport system, (4) a rubber granulate tank, (5) a polyurethane/binder tank, (6) a catalyst tank, and (7) a paint tank.

The tiles used in this work were made at a size of 1000 × 1000 × 10 mm. A total of 9 kg of rubber granulate, 380 g of binder (polyurethane STOBICOLL 352.00), and 5 g of catalyst (DABCO K 2097) were added to the bucket and mixed for 5 min using an industrial mixer (Figure 2).

Figure 2. Industrial mixer.

The listed ingredients were brought to the bucket using the material transport system. The catalyst was dosed with a pump and, depending on the weather conditions, it increased/decreased. After mixing, the mixture was placed into a pressing mold (Figure 3), evenly distributed, and pressed under a high temperature (120 °C) for 4 min.

Figure 3. Press mold.

After 4 min, the tile was taken out of the mold and placed on its side to cool. Recycled rubber tiles are mostly composed of 20% of granules of a size 0.5–2.0 mm and 80% of granules of a size 2.0–3.5 mm. The final product is shown in Figure 4.

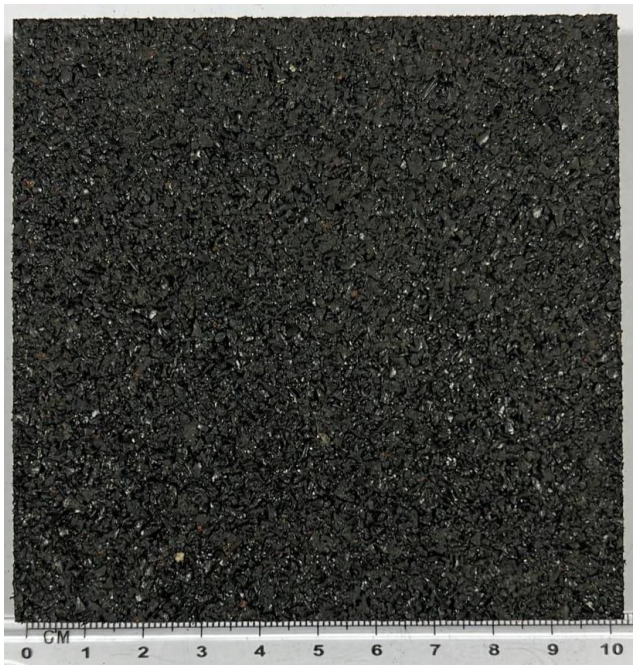

Figure 4. Recycled rubber tile.

In addition to the black rubber tiles, green and red rubber tiles were obtained for the experiments since colored rubber tiles are often used on children's playgrounds. Depending on the customer's wishes, needs, and the purpose of a certain granulate, the granules can be colored red, green, blue, or white, etc. Of course, coloring also increases the value of the product. The paints were stored in the paint tank and, depending on need, dosed using a pump.

2.1.1. Rubber Substrates Pre-Preparation

The recycled rubber substrate was first etched with a sodium hydroxide solution (NaOH, 1:10, w:V) according to the procedure described in [25] to make the surface as rough as possible and to form -OH groups in order to achieve the binding of the TiO_2 photocatalyst on the rubber surface using the sol–gel method. The NaOH solution was prepared from granules (NaOH, Lachner, Neratovice, Czech Republic) with deionized

water. Before soaking the rubber tiles into the prepared solution, the tiles were weighed and washed with ethanol (96%, Gram-mol), after which they were air-dried for 10 s. Afterwards, tiles were soaked in the NaOH solution for 40 min, after which they were washed with deionized water and dried for 24 h at 60 °C.

2.1.2. Photocatalyst Immobilization by the Sol–Gel Method

The photocatalyst TiO_2 (Evonik, Essen, Germany, Aeroxid®, TiO_2 P25, 30 nm, 56 m^2/g, 75:25 anatase–rutile mass ratio) was immobilized on the rubber substrates using the sol–gel method described in [26]. Three sets of experiments were conducted with black rubber tiles. Different proportions of TiO_2 were added to the sol–gel solution and were functionalized with appropriate amounts of tetraethyl orthosilicate (TEOS, ≥99.9% Sigma-Aldrich, Steinheim, Germany); 2 g TiO_2/5 mL TEOS, 4 g TiO_2/10 mL TEOS, and 10 g TiO_2/20 mL TEOS.

The sol–gel solution (the most perspective) was prepared by mixing 2 g of TiO_2, 200 mL of deionized water, and 200 mL of ethanol (GramMol, 96%), followed by 10 min of stirring and a 3 min treatment in an ultrasonic bath. When the solution was well-stirred, 70 mL of acetic acid (99–100% p.a., LabExpert, Ljubljana, Slovenia) was added to adjust the pH to an acidic level of approximately 3–4. For better binding, 5 mL of TEOS was added to the solution. Afterwards, the solution was stirred at 50 °C for 1 h. The rubber substrates were soaked in a prepared solution for 10 min and then dried at 80 °C for 20 min. The soaking procedure was performed four times in a row, and the substrates were then left for one week at room temperature. The same procedure was used for samples with 4 g TiO_2/10 mL TEOS and 10 g TiO_2/20 mL TEOS.

Red and green rubber substrates were immobilized with the most perspective TiO_2 mass proportion, based on the obtained results with black rubber substrates.

2.2. Characterization of Rubber Substrates

2.2.1. Scanning Electron Microscopy (SEM) and Energy Dispersion Spectroscopy (EDS)

The characterization of the immobilized layer in terms of crystal structure and morphology was investigated by SEM. SEM was performed with scanning electron microscopy using an FEG SEM Quanta 250 FEI microscope operating at 20 kV and a working distance set at 20 mm under low vacuum conditions ("as is") without evaporation. EDS mapping was performed using an EDS detector, Oxford Pentafet. To select the best ratio of TiO_2 immobilization (2, 4, or 10 g), each sample was cut into three layers to determine how deep the TiO_2 had entered into the substrate. Three layers were horizontally cut at 2 mm, 4 mm, and 6 mm of height from the surface.

2.2.2. Fourier Transform Infrared Spectroscopy (FTIR)

FTIR was performed using a Bruker Vertex 70 in ATR (attenuated total reflectance) mode. The samples were pressed on a diamond. The absorbance data were collected between 400 and 4000 cm^{-1} with a spectral resolution of 1 cm^{-1} and 64 scans. The equipment was sourced from Bruker Corporation, Billerica, MA, USA.

2.3. Leaching Test

The possible leaching of tire constituents into the environment and their subsequent potential adverse impact is of great concern for recycling and reusing waste tires [27]. To simulate natural leaching in a laboratory, a leaching test was used [28] to quantify the leaching of hazardous substances from media into groundwater and other water systems. These tests have been standardized by international agencies such as the International Organization for Standardization (ISO) because their results can provide important information for understanding and addressing human health risks from contaminated soil [29]. Various methods are available, but a selection that can precisely simulate the real-life scenario is challenging. Moreover, none of the laboratory leaching tests can replace the leaching behavior of materials in nature. Nevertheless, when used within the proper framework, the leaching test can ensure helpful information for environmental decision-making [28].

According to evaluation, several countries and agencies have standardized leaching test methods [29]. This paper reviews a tire–water chemical interaction based on the author's research. Due to the metals and textiles present in tires, heavy metals are expected to be found. In this work, the samples were sliced and leached for 24 h with deionized water with a liquid/sample ratio (L/S) of 1/10. The leachates were then recovered by filtering the eluate through a 0.45 µm filter. The TDS (Total Dissolved Solids) were analyzed on Hach Lange Sension 156 multimeter and DOC (dissolved organic carbon) was analyzed on a Shimadzu TOC/TN analyzer. Chlorides, fluorides, and sulphates were analyzed on a Hach Lange DR 5000 spectrophotometer. Metals were analyzed on a PerkinElmer AAnalyst 800 spectrometer. The analysis was performed using three techniques: the flame technique (FAAS) for the elements zinc (Zn), chromium (Cr), and copper (Cu); the graphite technique (GFAAS) for arsenic (As), barium (Ba), cadmium (Cd), molybdenum (Mo), nickel (Ni), lead (Pb), selenium (Se), silicon (Si), and titanium (Ti); and the hydride technique (FIAS) for mercury (Hg) only. The results of the test were compared with the ordinance on the methods and conditions for the landfill of waste, categories and operational requirement for landfills [30], and the Toxicity Characteristic Leaching Procedure (TCLP) [31].

For the comparison with the limit values of eluate parameters in the ordinance on the methods and conditions of waste disposal categories and the operating conditions for landfills, due to the differences in the unit reporting, the conversion of measured leaching concentrations was performed in correspondence with the following conversion formula (Equation (1)) [32]:

$$\text{Leached substance [mg/kg]} = \text{leaching concentration [mg/L]} \times \text{L/S ratio (L/kg)}, \quad (1)$$

2.4. Photocatalytic Oxidation Testing Set Up

The photocatalytic activity of the most perspective rubber tiles with immobilized TiO_2 was tested in preliminary experiments. The degradation of ammonia (NH_3) in the air stream was tested in the semi-pilot photocatalytic wind tunnel (PWT) shown in Figure 5. The flow-through reactor PWT resembles a solar simulator and can therefore be used for the testing of new photocatalytic materials such as photocatalytic rubber tiles. The reactor is made from a high-quality plexiglass material (thermoplastic, polymethyl methacrylate (PMMA)) consisting of two chambers separated by a screen with three slots for directional ventilation. The reaction chamber where photocatalytic tests are performed is followed by the measuring chamber. Rubber tiles were placed in the reaction chamber at a 10 cm distance from the irradiation source and positioned parallel to the air flow. In each experiment, there were four similar tiles (100 × 100 mm) in the reaction space, giving a total irradiated surface of 0.04 m^2. The PWT has one inlet connected to the source of NH_3, i.e., an aqueous solution with $c(0)NH_{3,aq}$ = 200 ppm. The air flow was achieved using the air pump with a maximum velocity of 3.4 m/s placed before the NH_3 source. Arduino sensors for temperature and humidity were placed in the measuring chamber, and an outlet was attached to a rinse. The reaction chamber was covered with the irradiation emission panel. The panel contained three irradiation sources simulating solar spectra with a higher-UVB to average-spectra ratio: Sunlight Pro Compact UV-B 2.0 23 W (Trixie), Compact UV Sun 20 W (Lucky Reptile), and Compact Pro 8.0 UVB 23 W (Terra Exotica) [15]. The incident irradiation intensities (I0, W m^{-2}) at the surface of the tiles were 13.3 and 24.6 for UVA and UVB irradiation, respectively, with >98% accuracy. Measurements were made with a UVP UVX radiometer following the previously established procedure [15].

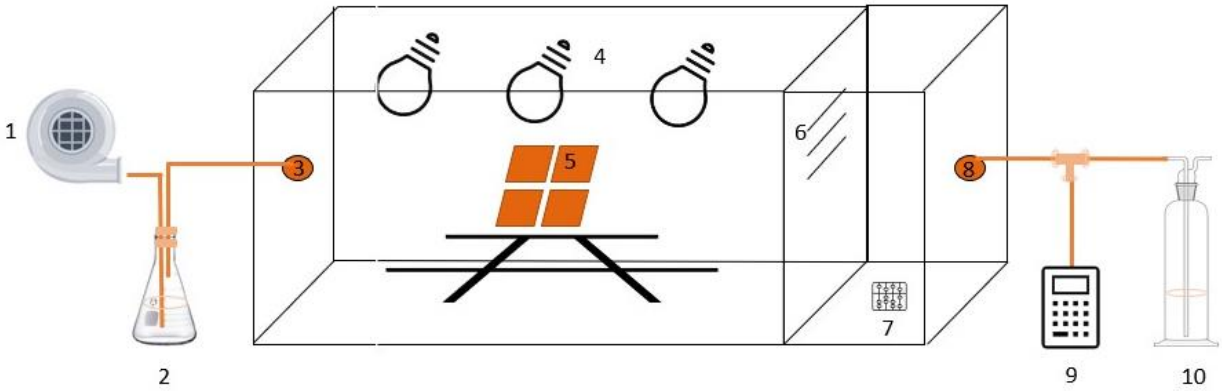

Figure 5. The reaction mechanism of experimental inquiry: (**1**) air pump; (**2**) Erlenmeyer flask with an aqueous ammonia solution; (**3**) inlet; (**4**) irradiation emission panel; (**5**) rubber tiles; (**6**) compartment with three ventilation slots; (**7**) Arduino sensor for temperature and humidity; (**8**) outlet; (**9**) gas analyzer; and (**10**) rinse.

Several sets of experiments were performed to determine the extent of NH_3 degradation in the PWT over rubber tiles with immobilized TiO_2. Referent experiments were performed with irradiated rubber tiles (without immobilized TiO_2) and in the dark to obtain the baseline of the NH_3 concentration and respective residence time in the PWT. The adsorption of NH_3 on the rubber tiles was studied in dark both with the referent rubber tiles and those with immobilized TiO_2. The photocatalytic experiments were performed with the rubber tiles with immobilized TiO_2 under irradiation. The duration of one experiment was 5 h. The continuous monitoring of gases CO, CO_2, NO_x, NO, NO_2, HC, and H_2S was conducted using a gas analyzer Testo 350 and a landfill gas analyzer GA5000 (Geotech, Leamington spa, Warwickshire, UK) for the monitoring of NH_3.

3. Results and Discussion

3.1. Rubber Substrates Pre-Preparation and Sol–Gel Immobilization

While the solution was clear and pure at the beginning of the 40-min process of pre-preparation, it became mucous and yellowish at the end. After 24 h of drying, the substrates were weighed. It was assumed that the weight increase was observed due to the formation of -OH groups on the substrate's surface (Table 1).

Table 1. Weighing results of samples (g).

2 g TiO_2			4 g TiO_2			10 g TiO_2		
Treatment NaOH		Sol–Gel	Treatment NaOH		Sol–Gel	Treatment NaOH		Sol–Gel
Before	After		Before	After		Before	After	
86.7	87.3	88.9	92.4	92.3	96.1	87.1	87.3	89.1
91.2	91.5	92.4	87.4	87.4	94.7	90.1	90.7	93.6
94.6	94.9	96.9	87.2	87.7	98.4	91.0	91.0	93.8
100.7	101.1	103.8	92.6	92.8	94.5	97.9	98.4	99.8
82.1	82.3	84.4	87.4	87.7	90.0	89.4	89.2	91.7
85.5	85.9	87.1	92.3	92.4	95.5	82.5	82.8	85.5

Additionally, the weighing of the rubber substrates was repeated after the sol–gel immobilization of TiO_2. The results are shown in Table 1.

An increase in the mass due to the sol–gel coating is evident, indicating the TiO_2 immobilizes on the surface of the rubber substrates.

3.2. Morphology of Rubber Substrates with Immobilized TiO_2

First, the addition of TiO_2 to rubber substrates—apart from impacting the rubber composition—affects the visual appearance of the rubber substrates, as can be seen in Figure 6. The dimensions of the tiles shown in Figure 6 are approximately 10 × 10 cm, as mentioned above in Figure 4. By comparing the referent black rubber substrate (a) with the three new samples (b–d), one can conclude that a higher proportion of TiO_2 results in higher surface coverage and, therefore, a visually whiter surface.

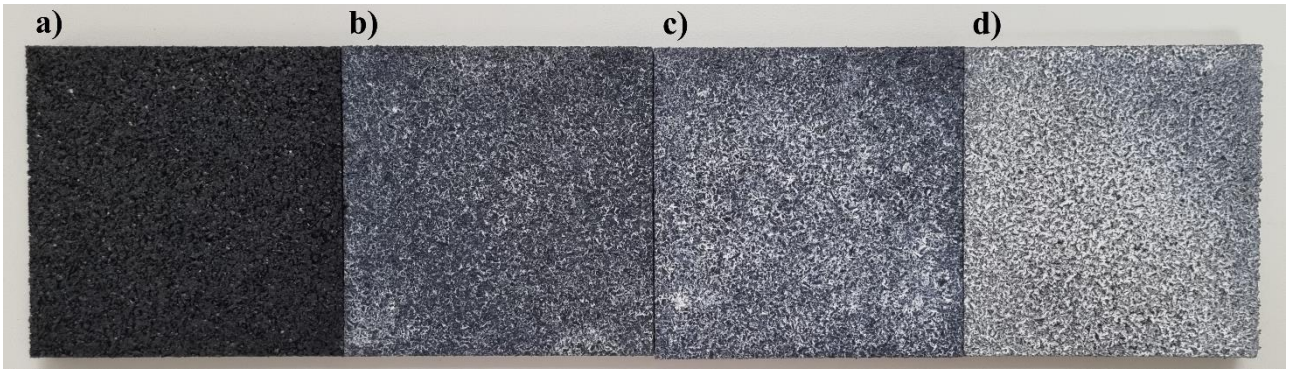

Figure 6. Surface comparison of referent rubber with sol–gel immobilized substrates: (**a**) referent substrate, (**b**) substrate with 2 g of TiO_2, (**c**) substrate with 4 g of TiO_2, and (**d**) substrate with 10 g of TiO_2.

3.2.1. SEM Analysis of Black Rubber Substrates with 2, 4, and 10 g of TiO_2

The SEM results of 100× microscopic magnification are shown in Figure 7. Figure 7a represents a sample of black referent rubber, while Figure 7b–d represent the TiO_2 immobilized by the sol–gel method with different mass proportions of TiO_2 (2, 4, and 10 g). By comparing results in Figure 7a–d, it is clear that TiO_2 has been immobilized on all rubber substrates.

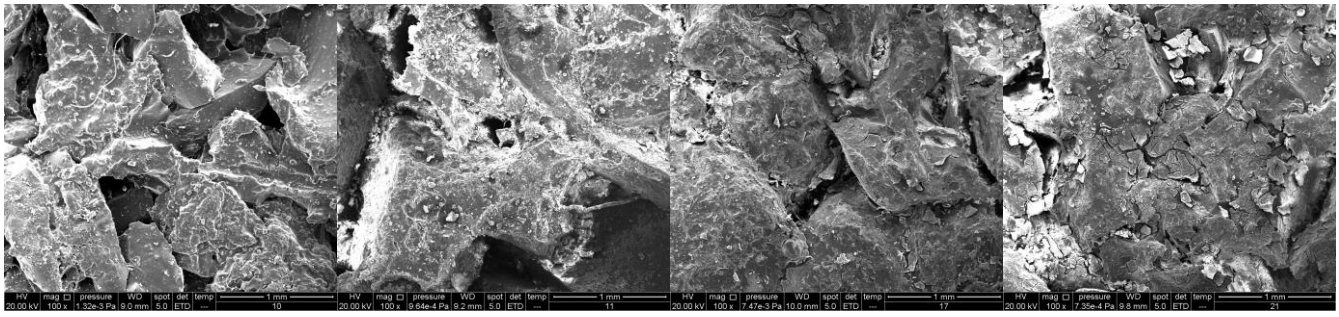

(**a**) (**b**) (**c**) (**d**)

Figure 7. Morphology of the black rubber substrates surfaces with different mass proportions of immobilized TiO_2 compared with the referent (100×): (**a**) referent rubber; (**b**) 2 g of TiO_2; (**c**) 4 g of TiO_2; and (**d**) 10 g of TiO_2.

As was previously mentioned, a surface coating was observed on samples with 4 and 10 g of TiO_2, but the amount of photocatalysts and binders caused the hardening of the surface layer and the formation of crusts. In this case, the crust may crack and TiO_2 may leach from the surface. The surface layer wears out given that the tiles are used for different purposes, so it is important that TiO_2 is present in the deeper layers as well.

3.2.2. SEM/EDS Analysis of Black Rubber Substrates with 2 g of TiO_2 through Horizontal Layer Analysis

According to the SEM/EDS analysis, immobilization with 2 g of TiO_2 was the most successful. Particles of TiO_2 were found in the deepest parts of the substrate. As is shown

in Figure 8, the presence of TiO_2 particles can be observed in all three layers (2, 4, and 6 mm).

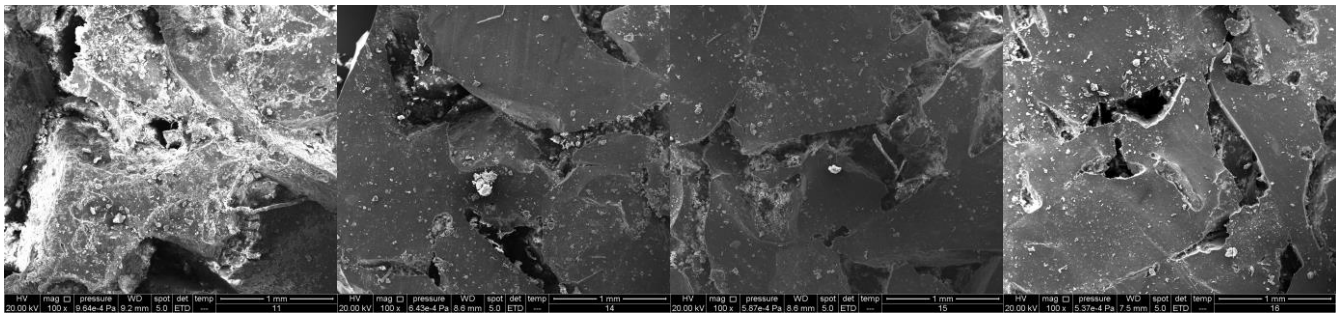

(**a**) (**b**) (**c**) (**d**)

Figure 8. Morphology of black rubber substrate with immobilized 2 g of TiO_2 through three horizontal layers (100×): (**a**) surface; (**b**) first layer (2 mm); (**c**) second layer (4 mm); and (**d**) third layer (6 mm).

Additionally, EDS mapping was performed to determine which elements are detected in the rubber layers. The reference black rubber substrate (Figure 9) results showed the highest proportion of carbon—71.20 wt%, which was expected due to the characteristics of rubber material. Iron and zinc were also found due to the galvanized iron casing that contains car tires, but in a slightly lower mass fraction (Fe—1.23 wt% and Zn—3.46 wt%). Furthermore, the mass concentration of oxygen was 24.11 wt%.

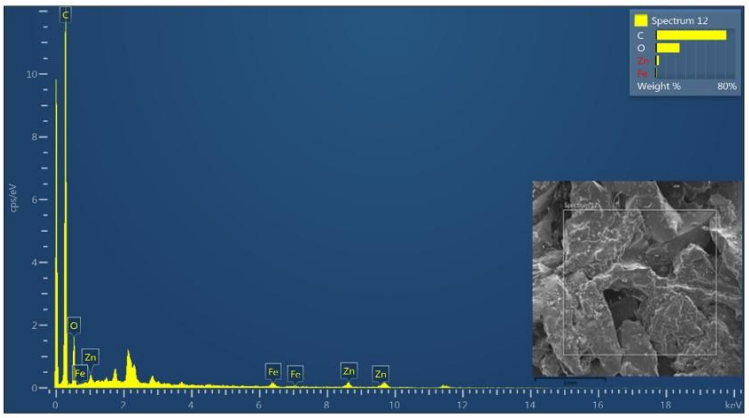

Figure 9. EDS mapping of the reference black rubber substrate (100×).

During the separation of the casing and the subsequent crushing of the rubber, a small, insignificant amount of these elements remained present in the raw material [33].

For comparison, an EDS mapping was performed on the sample's deepest layer, in which 2 g of TiO_2 was immobilized (Figure 10). It is important to note that titanium particles were present in this layer, confirming the successful penetration and immobilization of TiO_2 into deeper layers with a mass concentration of 0.74 wt%. Accordingly, the presence of TiO_2 on the surface was also confirmed in the first and second layers. In addition to the presence of Ti, EDS mapping showed that the following elements were present in this sample in the following mass concentrations: C—69.83 wt%, O—18.68 wt%, Na—2.33 wt%, Si—3.45 wt%, and Zn—4.97 wt%. Two new elements, sodium and silicon, were found in this sample. Na was the result of etching the rubber with the NaOH solution, while Si was the result of using TEOS.

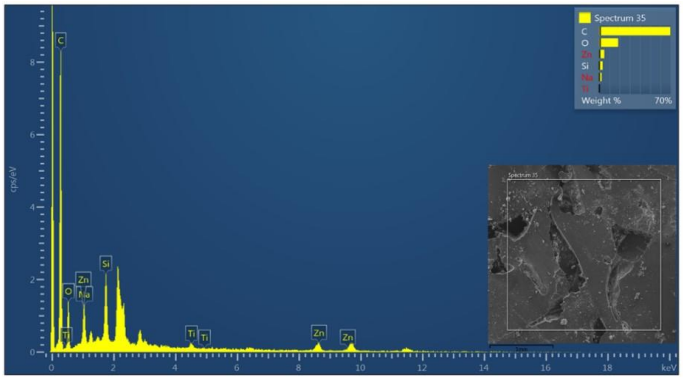

Figure 10. EDS mapping of TiO_2 (2 g) immobilization on black rubber substrate (100×) in the third layer.

The SEM/EDS analysis of substrates with 4 and 10 g showed that TiO_2 particles did not enter into deeper layers of the rubber substrate. Therefore, further analysis of the given substrates was not considered.

3.2.3. SEM/EDS Analysis of Red and Green Rubber Substrates with 2 g of TiO_2 through Horizontal Layer Analysis

The results of the SEM analysis showed that the immobilization of TiO_2 with the lowest content (2 g) was the most successful for the black rubber tile. Therefore, samples of colored rubber were made only with the lowest content of TiO_2 (Figure 11) and characterized accordingly. The procedure was the same for the rubber preparation and sol–gel solution, and the colored rubber substrates behaved the same as the black reference ones.

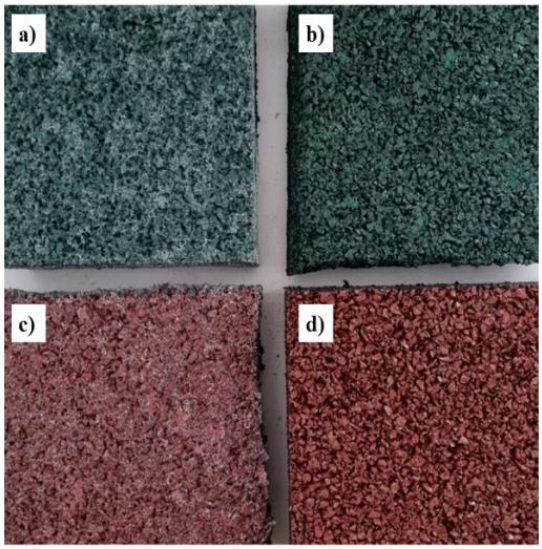

Figure 11. Surface comparison of referent rubber with sol–gel immobilized substrates: (**a**) green substrate with 2 g of TiO_2, (**b**) referent green substrate, (**c**) red substrate with 2 g of TiO_2, and (**d**) referent red substrate.

According to the SEM analysis, shown in Figure 12, EDS-confirmed TiO_2 particles were observed. Note that Figure 12a represents the surface of red rubber, while Figure 12b–d represent layers of different depths.

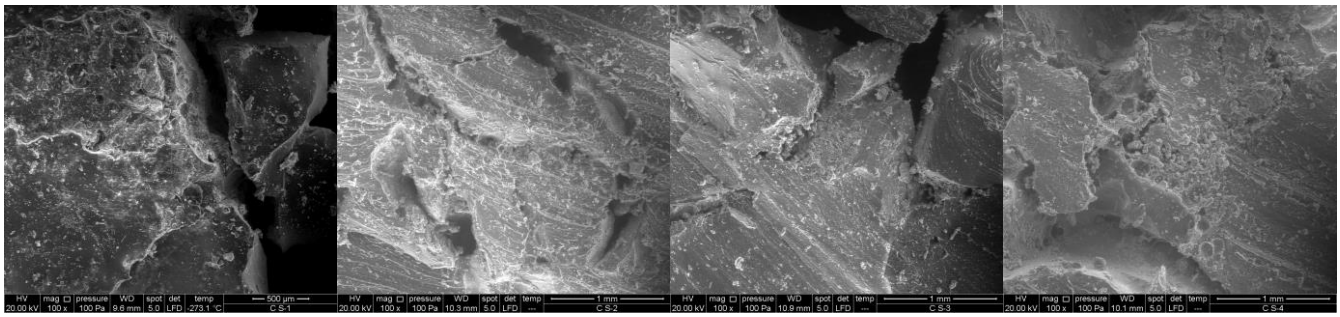

(**a**) (**b**) (**c**) (**d**)

Figure 12. Morphology of a red rubber substrate with an immobilized 2 g of TiO_2 through three horizontal layers (100×): (**a**) surface; (**b**) first layer (2 mm); (**c**) second layer (4 mm); and (**d**) third layer (6 mm).

The SEM/EDS analysis of green rubber substrates also showed the presence of titanium particles in the deeper layers of the sample, as is shown in Figure 13.

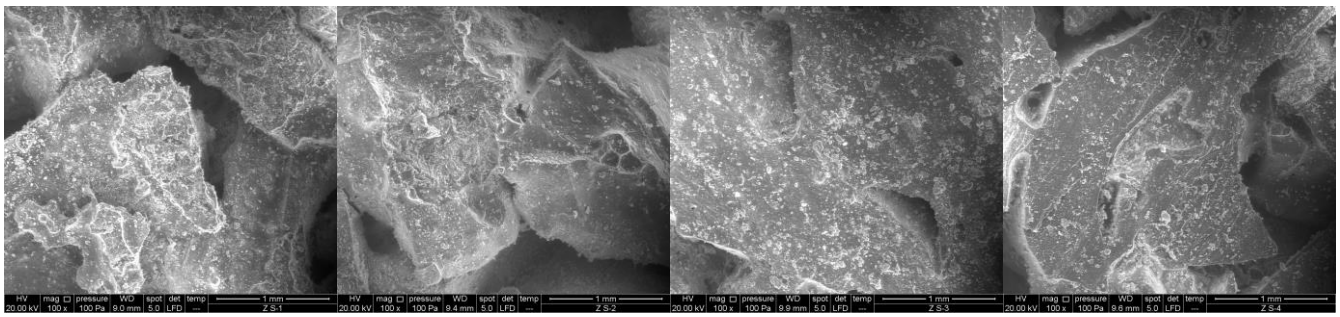

(**a**) (**b**) (**c**) (**d**)

Figure 13. Morphology of a green rubber substrate with an immobilized 2 g of TiO_2 through three horizontal layers (100×); (**a**) surface; (**b**) first layer (2 mm); (**c**) second layer (4 mm); and (**d**) third layer (6 mm).

3.3. FTIR Analysis of Rubber Substrates

The FTIR results were consistent for all the tested rubber tiles (black, green, and red). Figure 14A shows the FTIR absorption spectra in the range of 4000–2200 cm^{-1} of immobilized TiO_2 on referent black rubber (a), referent black rubber (b), and etched black rubber with the NaOH solution (1/10, w/V) (c). The absorption band at 3300 cm^{-1} on Figure 14 A(c), is attributed to the -OH bending and stretching vibrations, respectively [34,35], and is reduced (Figure 14A(a)) since the immobilization of TiO_2 on the rubber was performed by the sol–gel method through reactions with -OH groups.

In the Figure 14B(a), the absorption band around 1215 cm^{-1} and 1100 cm^{-1} is attributed to the vibration bands of Si–O–Si groups [34,35], the shoulder at 800 cm^{-1} can be assigned to the symmetric stretching of the Si–O–Si [35], and the appearance of the overlapped band from 900 to 1000 cm^{-1} could be linked to the Ti–O–Si bonds superimposed on the stretching vibrations of the Si–O or Si-OH groups [36]. Furthermore, the band near 950 cm^{-1} refers to the stretching vibration of the Ti-O-Si groups [34,35,37]. The band around 1440 cm^{-1} in Figure 14B(c) can be assigned to the reaction of copper (II) oxide (CuO), a coloring pigment for green rubber, and the formed -OH groups [38].

All the FTIR results confirmed that titanium was successfully bound to the OH groups that were formed after pre-treatment with NaOH. Likewise, the Ti-O-Si connection shows us that titanium (Ti) was successfully connected to silicon (Si) by the sol–gel method that led to the successful immobilization.

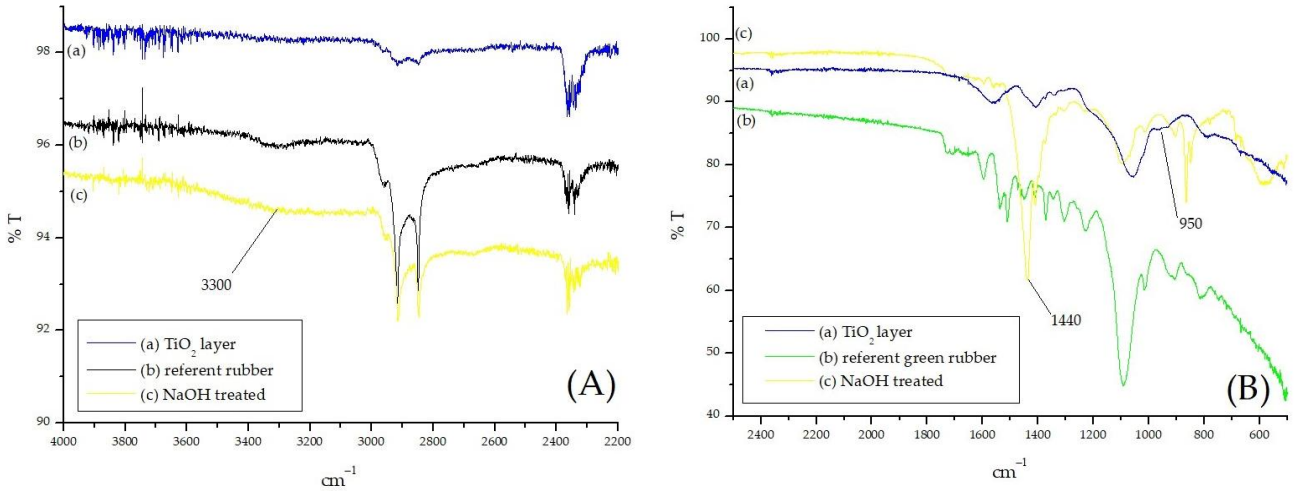

Figure 14. (**A**) FTIR spectra in the range of 4000–2200 cm^{-1} of (**a**) immobilized TiO_2 on referent black rubber, (**b**) referent black rubber, and (**c**) etched black rubber with NaOH solution; (**B**) FTIR spectra in the range of 2500–500 cm^{-1} of (**a**) immobilized TiO_2 on referent green rubber, (**b**) referent green rubber, and (**c**) etched green rubber with NaOH solution.

3.4. Leaching Test Analysis

3.4.1. Black Rubber Substrates (2 g)

Prior to and after the leaching test, samples were weighed (Table 2). The mass of the referent and sample with TiO_2 is slightly less than the initial one, indicating the rinse of the photocatalyst surface.

Table 2. Weighing results of samples of black rubber before and after the leaching test.

	Weight at the Beginning [g]	Weight at the End [g]
Referent black	7.0172	7.0088
2 g TiO_2	8.8976	8.8120

Comparison with the given limit values of both ordinances [30,31] stated in Section 2.3 showed that the results of As, Ba, Cd, Cr, Cu, Hg, Mo, Ni, Pb, and Se for the referent black rubber sample and the sample with TiO_2 were below their respective regulatory limits (Table 3). An increase in Cd concentration from <0.002 µg/L (detection limit) to 2.09 µg/L and a Mo concentration from 1.22 µg/L to 2.94 µg/L was noticed after immobilization TiO_2. Despite the observed increase, the given values are under regulatory limits [30,31].

Furthermore, the initial concentration of Zn was 7.3 mg/kg, but after sol–gel immobilization it was 732 mg/kg, which exceeds the maximum permissible limit value given by the ordinance [30]. As one of the highest-concentration compounds typical in waste tires, zinc is not categorized as a hazardous material in the TCLP limits [31,33]. The presence of zinc comes from the galvanized iron castings originally found in tires. The same is proven in the EDS results in Figures 9 and 10.

The Si and Ti are not regulated; nevertheless, they were of interest to observe (Table 3) in terms of the photocatalytic-layer contribution to the leaching. The Si concentration increased from 1472.6 µg/L to 2216.0 µg/L due to the usage of TEOS in the sol–gel preparation, while the Ti concentration decreased from 26.09 µg/L to <0.35 µg/L (detection limit). Given results indicate the efficient immobilization of TiO_2. The Si content indicates that the amount of TEOS used in the sol–gel could be decreased. Since Ti is found in a certain concentration, it would be desirable to know the maximum permissible concentration of Ti, although it is not regulated according to [30] and [31]. Additionally, according to [39], no normative references were found on the permissible limits for Ti concentration. Regarding its toxicity in water, the European Chemicals Agency (ECHA, 2022) states that TiO_2 is not

acutely or chronically toxic to aquatic organisms. Concerning sediments, it appears to have a low potential for acute and chronic freshwater and marine sediment toxicity based on the data available for insect, crustacean, and annelid species. Regarding terrestrial toxicity, data indicate that TiO_2 is not toxic to soil organisms, including microbes, plants, and invertebrates up to at least 1000 mg/kg dw soil. According to the above, we can conclude that the Ti concentrations obtained in our research will not impact the environment [40].

Table 3. Results of leaching test for black rubber.

Parameter	Unit	Referent (Black)	2 g TiO_2
As	µg/L	<0.05	<0.05
Ba	µg/L	<0.35	<0.35
Cd	µg/L	<0.002	2.09
Cr	mg/L	<0.003	<0.003
Cu	mg/L	<0.0015	<0.0015
Hg	µg/L	<0.009	<0.009
Mo	µg/L	1.22	2.94
Ni	µg/L	<0.07	<0.07
Pb	µg/L	<0.05	<0.05
Se	µg/L	<0.05	<0.05
Zn	mg/L	0.73	72.3
Si	µg/L	1472.6	2216.0
Ti	µg/L	26.09	<0.35
Cl^-	mg/L	2.1	7.4
F^-	mg/L	0.12	1.02
SO_4^{2-}	mg/L	1	3
DOC	mg/L	39.5	487.5
TDS	mg/L	13.4	514

Moreover, chlorides, fluorides, and sulphates were below their maximum prescribed values [30], although a slight increase in their values has been observed (Table 3).

The DOC concentrations before TiO_2 application were 395 mg/kg. They were 4875 mg/kg after the application, which is a result of the attachment of residual organic forms in the sol–gel process. The significant increase of DOC exceeds the maximum prescribed value of 3000 mg/kg (Table 3) according to [30]. The concentration of TDS also increased for the same reason as the DOC concentration, but was still within the prescribed limits (Table 3) [30].

3.4.2. Red Rubber Substrates (2 g)

The leaching for referent red samples and samples with TiO_2 showed that the metals As, Ba, Cd, Cr, Cu, Hg, Mo, Ni, Pb, and Se were below their respective regulatory limits according to both ordinances [30,31]. The results show a slight increase after TiO_2 immobilization in As, Cd, and Mo concentrations, shown in Table 4. The concentration of Zn was 1.10 mg/L, and it was 41.6 mg/L after TiO_2 immobilization. According to the prior observed results from the black rubber substrates, this was expected. According to the regulatory limits of the ordinance [30] after the conversion of the units, the given value of Zn in the red rubber sample after immobilization was 416 mg/kg, which is higher than the allowed maximum concentration.

The concentration of Si increased from <1.0 µg/L to 3118 µg/L due to TEOS used in the sol–gel preparation. On the other hand, the Ti concentration before and after immobilization was <0.35, representing the detection limit (Table 4). The black rubber sample showed the same results. According to the results obtained with the black rubber, we can also conclude that the Ti concentrations obtained by our research will not affect the environment [40].

The anions in the red rubber samples were below the maximum limit [30], and a slight increase can be seen in Table 4.

Table 4. Results of leaching test for red rubber.

Parameter	Unit	Referent	2 g TiO_2
As	µg/L	<0.05	0.073
Ba	µg/L	<0.35	<0.35
Cd	µg/L	<0.002	0.43
Cr	mg/L	<0.003	<0.003
Cu	mg/L	<0.0015	<0.0015
Hg	µg/L	<0.009	<0.009
Mo	µg/L	1.89	3.7
Ni	µg/L	<0.07	<0.07
Pb	µg/L	<0.05	<0.05
Se	µg/L	<0.05	<0.05
Zn	mg/L	1.1	41.6
Si	µg/L	<1.0	3118
Ti	µg/L	<0.35	<0.35
Cl^-	mg/L	3	9.5
F^-	mg/L	<0.02	0.55
SO_4^{2-}	mg/L	0	2
DOC	mg/L	17.83	286.2
TDS	mg/L	15.2	396

The DOC concentrations prior to the immobilization were 178.3 mg/kg and 2862 mg/kg after the immobilization, which is below the maximum limit (Table 4) [30]. This is the result of the attachment of residual organics from the sol–gel process. The concentration of TDS also increased, but was still within the allowable limits (Table 4) [30].

3.4.3. Green Rubber Substrates (2 g)

As with previous results, the concentration of As, Ba, Cd, Cr, Cu, Hg, Mo, Ni, Pb, and Se were below the maximum allowable limits [30,31]. A slight increase in concentration after the immobilization of TiO_2 was observed in Cd and Mo, as well as in the black rubber samples. The Zn concentration before and after immobilization was still above the maximum limit (Table 5) [30].

Table 5. Results of leaching test for green rubber.

Parameter	Unit	Referent	2 g TiO_2
As	µg/L	<0.05	<0.05
Ba	µg/L	<0.35	<0.35
Cd	µg/L	<0.002	0.29
Cr	mg/L	<0.003	<0.003
Cu	mg/L	<0.0015	<0.0015
Hg	µg/L	<0.009	<0.009
Mo	µg/L	1.67	2.25
Ni	µg/L	<0.07	<0.07
Pb	µg/L	<0.05	<0.05
Se	µg/L	<0.05	<0.05
Zn	mg/L	0.56	35.8
Si	µg/L	1074.0	2744
Ti	µg/L	25.87	<0.35
Cl^-	mg/L	2.6	6.5
F^-	mg/L	0.06	0.87
SO_4^{2-}	mg/L	1	1
DOC	mg/L	24.74	201
TDS	mg/L	18.4	294

The Si concentration increased from 1074 µg/L to 2744 µg/L due to the TEOS in the sol–gel preparation (Table 5). The Ti concentration decreased from 25.87 µg/L to

<0.35 µg/L (detection limit), as in the black rubber samples. When comparing the black and red samples, we can conclude that the Ti concentrations obtained by our research will not affect the environment when all samples are considered

Chlorides and fluorides were below their maximum prescribed values [30], although a slight increase in values was observed (Table 5). Sulphates were also below the maximum limits [30], but their concentration was the same in the referent green rubber sample and the sample with TiO_2.

The DOC concentrations before TiO_2 application were again 247.4 mg/kg and 2010 mg/kg after the application, below the maximum limit (Table 5) [30]. The concentration of TDS also increased but is still within the prescribed limits (Table 5) [30].

3.5. Photocatalytic Oxidation of NH_3 over Rubber Tiles with 2 g TiO_2 Immobilized

According to the characterization results, rubber tiles with the addition of 2 g of TiO_2 have shown to be the most perspective. The results of the NH_3 photocatalytic oxidation testing on black rubber tiles are presented in Figure 15.

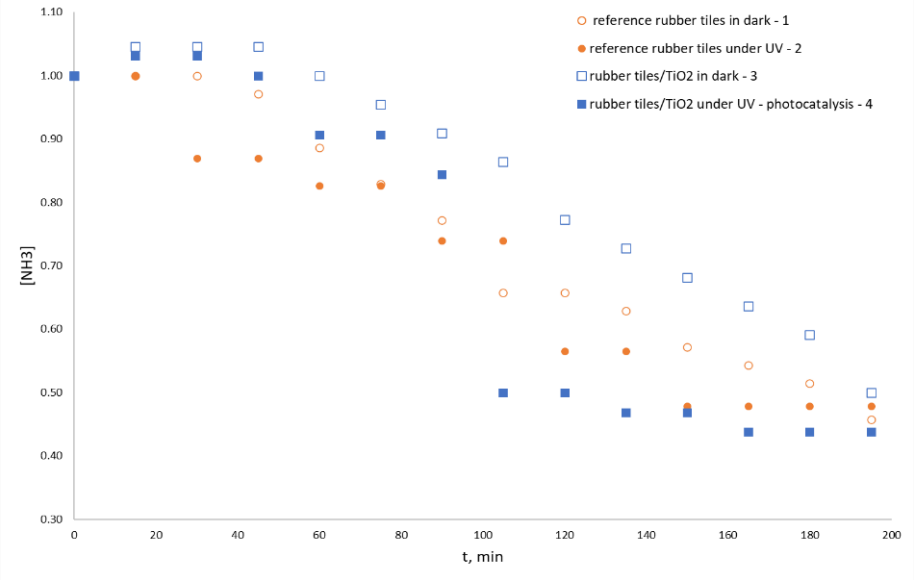

Figure 15. Measured concentration of NH_3 at the outlet of the PWT reactor during experiments.

In comparison to the modified rubber tiles (Figure 15—3 and 4), the NH_3 degradation kinetics during the referent experiments (Figure 15—1 and 2) can be explained by the adsorption of NH_3 on rubber tiles. Adsorption is more noticeable on the referent rubber tiles due to the porosity of the rubber material and the tendency of gases to fill the cavities. When TiO_2 is immobilized on tiles, a certain portion of the tiles' surface and cavities is occupied by TiO_2, imposing mass-transfer limitations on NH_3 diffusion and adsorption. The latter results in the higher-measured NH_3 concentrations in the dark after passing over the modified rubber tiles. Moreover, a decrease in the NH_3 concentrations during the referent experiment over irradiated rubber tiles point at the wet catalytic oxidation of the NH_3 in the presence of humidity and temperature, due to presence of possible catalytic centers (i.e., metals) in recycled rubber.

To estimate the NH_3 oxidation extents relative to the general trend of NH_3 decrease in the PWT during time span (a baseline), kinetics were studied and experimental reaction rates in the PWT were determined (Table 6).

Table 6. Experimentally determined rates of NH_3 content decrease in the PWT.

Experimental Setup in the PWT		Rate of NH_3 Decrease [ppm min^{-1}]
Material	**Irradiation**	
None *	NO	0.0538
Recycled rubber tiles (referent)	NO	0.0750
Recycled rubber tiles (referent)	YES	0.0826
Modified rubber tiles (with TiO_2)	NO	0.0581
Modified rubber tiles (with TiO_2)	YES	0.0935

* Data not shown graphically.

Given numbers suggested the favorable adsorption of NH_3 on recycled rubber tiles due to relatively higher rates of NH_3 decrease, while the adsorption of NH_3 on TiO_2 surface in the dark was insignificant. This is in accordance with the previous findings. Namely, it was assumed that only a weak physical adsorption occurs in dark and is followed by a fast desorption when irradiation starts, hence the increase in the NH_3 concentration in the outlet in the case of the irradiated photocatalyst during the first minutes of the process [15]. As expected, the rate of the NH_3 decrease was the highest in the case of the modified rubber tiles (with TiO_2). Having weak adsorption in mind, one can conclude that only the oxidation reaction is responsible for the observed decrease. The estimated photocatalytic extent was 1.60 times higher that adsorption alone, while it was 1.13 times higher than oxidation over the referent recycled rubber.

The direct oxidation of NH_3 to N_2 was observed during photocatalytic oxidation of NH_3, as well as [15]. There were no NO_x or other unexpected gases detected at the outlet. Nonetheless, the presence of CO and H_2S were detected in the referent experiment with the irradiated rubber tiles, indicating that rubber loses its properties due to ageing. The presence of the TiO_2 on the rubber tiles improves the rubber stability under solar irradiation.

In this work, we introduced a basic kinetic analysis based on experimental results. As the photocatalytic removal rate of NH_3 (as the main performance metric) is sensitively dependent on the operation conditions (e.g., catalyst mass, reaction time, light irradiance, etc.), future research will be directed toward the actual performance computation of reported materials. For instance, the reduction of CO_2 to CO was analyzed by using performance metrics such as quantum yield (QY), space–time yield (STY), figure of merits (FoM), turnover frequency (TOF), and turnover number (TON) [41–45]. This will be an initial point for a further in-depth analysis of NH_3 reduction toward N_2.

4. Conclusions

The existing rubber tiles obtained from granules were successfully modified by a surface application of an anatase/rutile thin film from commercial TiO_2 P25 by a modified sol–gel process using TEOS as an organic precursor (2 g TiO_2/5 mL TEOS, 4 g TiO_2/10 mL TEOS, and 10 g TiO_2/20 mL TEOS). The SEM and EDS analyses of black rubber substrates showed that the optimal immobilization was achieved using the lowest TiO_2 mass proportion (2 g TiO_2/5 mL TEOS). On the samples with 4 g TiO_2/10 mL TEOS and 10 g TiO_2/20 mL TEOS, a crust was formed that cracked, and there was no penetration of TiO_2 into the deeper layers. For this reason, these ratios were no longer used for further research.

The latter was confirmed by the SEM and EDS analyses of black rubber substrates by horizontal layer analysis, demonstrating the penetration and immobilization of the TiO_2 nanoparticles. The same penetration and immobilization were observed in the red and green rubber substrates.

The FTIR analysis has shown the formation of the wideband at 3300 cm^{-1}, which is attributed to -OH groups forming due to NaOH treatment. Furthermore, the bands at 950 and 800 cm^{-1}, assigned to the Ti–O–Si and Si–O–Si groups after NaOH pretreatment and TiO_2 immobilization, indicate that the immobilization of TiO_2 on the newly formed -OH groups was successful. The formation of chemical bonds could also explain the low-Ti content in the leachate.

The stability and environmental impact of rubber substrates (black, red, and green) were investigated by a leaching test. Leached substances were the results of the rubber composition. As was previously mentioned, the results related to the leached Ti concentration indicate an efficient immobilization of TiO_2. In contrast, Si concentrations assumed that the amount of TEOS used in the immobilization sol–gel method could be decreased, offering favorable start for the industrial development of modified rubber tiles.

Photocatalytic oxidation of NH_3 was achieved by using black rubber tiles immobilized with 2 g of TiO_2, confirming the photocatalytic oxidation of NH_3 to N_2. Furthermore, a decrease of NH_3 in the presence of irradiation during the referent experiment without TiO_2 layer indicates a possible wet catalytic oxidation which is a result of presence of metalloid particles in the rubber tiles. Therefore, the TiO_2 layer on rubber tiles contributes to the protection of the rubber tiles against typical wear due to atmospheric exposure, confirming the use of these new materials for passive air protection.

Based on the given results, rubber substrates with the addition of 2 g of TiO_2 have been shown to be the most perspective for further tests of air pollutant photocatalytic degradation.

Author Contributions: Conceptualization, P.B., L.R., I.B. and I.G.; methodology, P.B., I.B., M.T. and B.R.; software, B.R.; validation, I.G. and I.B.; formal analysis, I.B. and V.Š.; investigation, P.B.; resources, I.G.; data curation, P.B.; writing—original draft preparation, P.B.; writing—review and editing, P.B., L.R. and I.B.; visualization, P.B. and L.R.; supervision, I.G. and I.B.; project administration, I.G.; funding acquisition, I.G. All authors have read and agreed to the published version of the manuscript.

Funding: This work has been supported by the project, "Recycling rubber & solar photocatalysis: ecological innovation for passive air and health protection", supported by the European Regional Development Fund, KK.01.1.1.07.0058.

Data Availability Statement: Not applicable.

Acknowledgments: The authors would also like to acknowledge the Gumiimpex Ltd. company as the partner on the stated project and for providing the materials. This work has been supported by the Virtulab project (KK.01.1.1.02.0022) and was co-funded by the European Regional Development Fund.

Conflicts of Interest: The authors declare no conflict of interest. The sponsors had no role in the design, execution, interpretation, or writing of this study.

References

1. Formela, K. Sustainable development of waste tires recycling technologies—Recent advances, challenges and future trends. *Adv. Ind. Eng. Polym. Res.* **2021**, *4*, 209–222. [CrossRef]
2. Gumiimpex.grp. Available online: https://gumiimpex.hr/proizvodi-od-reciklirane-gume/ (accessed on 31 August 2022).
3. Huang, T.J.; Chang, L.T. Design and evaluation of shock-absorbing rubber tile for playground safety. *Mater. Des.* **2009**, *30*, 3819–3823. [CrossRef]
4. Vázquez, V.F.; Luong, J.; Bueno, M.; Terán, F.; Paje, S.E. Assessment of an action against environmental noise: Acoustic durability of a pavement surface with crumb rubber. *Sci. Total Environ.* **2016**, *542*, 223–230. [CrossRef] [PubMed]
5. Halsband, C.; Sørensen, L.; Booth, A.M.; Herzke, D. Car Tire Crumb Rubber: Does Leaching Produce a Toxic Chemical Cocktail in Coastal Marine Systems? *Front. Environ. Sci.* **2020**, *8*, 125. [CrossRef]
6. Šimun, M.; Mihalinac, S. Asphalt pavement surface course with recycled rubber. *Gradjevinar* **2019**, *71*, 639–650. [CrossRef]
7. Edil, T.B. A review of environmental impacts and environmental applications of shredded scrap tires. In *Scrap Tire Derived Geomaterials-Opportunities and Challenges: Proceedings of the International Workshop IW-TDGM 2007*; CRC Press: Boca Raton, FL, USA, 2008.
8. Mclintock, I.S.; Ritchie, M. Reactions on titanium dioxide; photo-adsorption and oxidation of ethylene and propylene. *Trans. Faraday Soc.* **1965**, *61*, 1007–1016. [CrossRef]
9. Peral, J.; Ollis, D.F. Heterogeneous photocatalytic oxidation of gas-phase organics for air purification: Acetone, 1-butanol, butyraldehyde, formaldehyde, and m-xylene oxidation. *J. Catal.* **1992**, *136*, 554–565. [CrossRef]
10. Lichtin, N.N.; Avudaithai, M.; Berman, E.; Grayfer, A. TiO_2-photocatalyzed oxidative degradation of binary mixtures of vaporized organic compounds. *Sol. Energy* **1996**, *56*, 377–385. [CrossRef]
11. Zhao, J.; Yang, X. Photocatalytic oxidation for indoor air purification: A literature review. *Build. Environ.* **2003**, *38*, 645–654. [CrossRef]
12. Stefanov, B.I.; Niklasson, G.A.; Granqvist, C.G.; Österlund, L. Gas-phase photocatalytic activity of sputter-deposited anatase TiO_2 films: Effect of (0 0 1) preferential orientation, surface temperature and humidity. *J. Catal.* **2016**, *335*, 187–196. [CrossRef]

13. Abou Saoud, W.; Assadi, A.A.; Guiza, M.; Bouzaza, A.; Aboussaoud, W.; Soutrel, I.; Ouederni, A.; Wolbert, D.; Rtimi, S. Abatement of ammonia and butyraldehyde under non-thermal plasma and photocatalysis: Oxidation processes for the removal of mixture pollutants at pilot scale. *Chem. Eng. J.* **2018**, *344*, 165–172. [CrossRef]
14. Pelaez, M.; Nolan, N.T.; Pillai, S.C.; Seery, M.K.; Falaras, P.; Kontos, A.G.; Dunlop, P.S.M.; Hamilton, J.W.J.; Byrne, J.A.; O'Shea, K.; et al. A review on the visible light active titanium dioxide photocatalysts for environmental applications. *Appl. Catal. B Environ.* **2012**, *125*, 331–349. [CrossRef]
15. Grčić, I.; Marčec, J.; Radetić, L.; Radovan, A.-M.; Melnjak, I.; Jajčinović, I.; Brnardić, I. Ammonia and methane oxidation on TiO_2 supported on glass fiber mesh under artificial solar irradiation. *Environ. Sci. Pollut. Res.* **2021**, *28*, 18354–18367. [CrossRef]
16. Younis, S.A.; Kim, K.H. Heterogeneous photocatalysis scalability for environmental remediation: Opportunities and challenges. *Catalysts* **2020**, *10*, 1109. [CrossRef]
17. Grčić, I.; Papić, S.; Brnardić, I. Photocatalytic Activity of TiO_2 Thin Films: Kinetic and Efficiency Study. *Int. J. Chem. React. Eng.* **2018**, *16*. [CrossRef]
18. Murugan, M.; Subasri, R.; Rao, T.N.; Gandhi, A.S.; Murty, B.S. Synthesis, characterization and demonstration of self-cleaning TiO_2 coatings on glass and glazed ceramic tiles. *Prog. Org. Coat.* **2013**, *76*, 1756–1760. [CrossRef]
19. Wang, Z.; Gauvin, F.; Feng, P.; Brouwers, H.J.H.; Yu, Q. Self-cleaning and air purification performance of Portland cement paste with low dosages of nanodispersed TiO_2 coatings. *Constr. Build. Mater.* **2020**, *263*, 120558. [CrossRef]
20. Bianchi, C.L.; Gatto, S.; Pirola, C.; Scavini, M.; Vitali, S.; Capucci, V. Micro-TiO_2 as a starting material for new photocatalytic tiles. *Cem. Concr. Compos.* **2013**, *36*, 116–120. [CrossRef]
21. Ke, S.; Cheng, X.; Wang, Q.; Wang, Y.; Pan, Z. Preparation of a photocatalytic $TiO_2/ZnTiO_3$ coating on glazed ceramic tiles. *Ceram. Int.* **2014**, *40*, 8891–8895. [CrossRef]
22. Balayeva, N.O.; Fleisch, M.; Bahnemann, D.W. Surface-grafted WO_3/TiO_2 photocatalysts: Enhanced visible-light activity towards indoor air purification. *Catal. Today* **2018**, *313*, 63–71. [CrossRef]
23. Hu, Z.; Xu, T.; Liu, P.; Oeser, M. Microstructures and optical performances of nitrogen-vanadium co-doped TiO_2 with enhanced purification efficiency to vehicle exhaust. *Environ. Res.* **2021**, *193*, 110560. [CrossRef]
24. Kovalevskiy, N.S.; Lyulyukin, M.N.; Selishchev, D.S.; Kozlov, D.V. Analysis of air photocatalytic purification using a total hazard index: Effect of the composite TiO_2/zeolite photocatalyst. *J. Hazard. Mater.* **2018**, *358*, 302–309. [CrossRef] [PubMed]
25. Nuzaimah, M.; Sapuan, S.M.; Nadlene, R.; Jawaid, M. Sodium hydroxide treatment ofwaste rubber crumb and its effects on properties of unsaturated polyester composites. *Appl. Sci.* **2020**, *10*, 3913. [CrossRef]
26. Malinowski, S.; Presečki, I.; Jajčinović, I.; Brnardić, I.; Mandić, V.; Grčić, I. Intensification of dihydroxybenzenes degradation over immobilized TiO_2 based photocatalysts under simulated solar light. *Appl. Sci.* **2020**, *10*, 7571. [CrossRef]
27. Selbes, M.; Yilmaz, O.; Khan, A.A.; Karanfil, T. Leaching of DOC, DN, and inorganic constituents from scrap tires. *Chemosphere* **2015**, *139*, 617–623. [CrossRef] [PubMed]
28. Tiwari, M.K.; Bajpai, S.; Dewangan, U.K.; Tamrakar, R.K. Suitability of leaching test methods for fly ash and slag: A review. *J. Radiat. Res. Appl. Sci.* **2015**, *8*, 523–537. [CrossRef]
29. Someya, M.; Higashino, K.; Imoto, Y.; Sakanakura, H.; Yasutaka, T. Effects of membrane filter material and pore size on turbidity and hazardous element concentrations in soil batch leaching tests. *Chemosphere* **2021**, *265*, 128981. [CrossRef]
30. Za, O.S.; Vrstama, Š.T. Ministarstvo Zaštite Okoliša i Prirode 3086. 2018. Available online: https://narodne-novine.nn.hr/clanci/sluzbeni/2015_10_114_2184.html (accessed on 15 September 2022).
31. USEPA-Method: 1311 Toxicity Characteristic Leaching Procedure (TCLP). In *Hong Kong Accredit. LOR*; 2011. Available online: https://www.iowadnr.gov/Portals/idnr/uploads/waste/swfact_tclpfactsheet.pdf (accessed on 15 September 2022).
32. Van der Sloot, H.A.; Van Zomeren, A.; Meeussen, J.C.; Hoede, D.; Rietra, R.P.; Stenger, R.; Lang, T.; Schneider, M.; Spanka, G.; Stoltenberg-Hansson, E.; et al. Environmental Criteria for Cement Based Products Phase I: Ordinary Portland Cement Phase II: Blended Cements and methodology for impact assessment. *Energy Res. Cent. Neth.* **2011**, *2011*, 224.
33. Bocca, B.; Forte, G.; Petrucci, F.; Costantini, S.; Izzo, P. Metals contained and leached from rubber granulates used in synthetic turf areas. *Sci. Total Environ.* **2009**, *407*, 2183–2190. [CrossRef]
34. Riazian, M.; Montazeri, N.; Biazar, E. Nano structural properties of TiO_2-SiO_2. *Orient. J. Chem.* **2011**, *27*, 903–910.
35. Brnardić, I.; Huskić, M.; Umek, P.; Grgurić, T.H. Sol-gel functionalization of sodium TiO_2 nanotubes and nanoribbons with aminosilane molecules. *Ceram. Int.* **2013**, *39*, 9459–9464. [CrossRef]
36. Brnardić, I.; Huskić, M.; Umek, P.; Fina, A.; Grgurić, T.H. Synthesis of silane functionalized sodium titanate nanotubes and their influence on thermal and mechanical properties of epoxy nanocomposite. *Phys. Status Solidi Appl. Mater. Sci.* **2013**, *210*, 2284–2291. [CrossRef]
37. Barkoula, N.M.; Alcock, B.; Cabrera, N.O.; Peijs, T. Flame-Retardancy Properties of Intumescent Ammonium Poly(Phosphate) and Mineral Filler Magnesium Hydroxide in Combination with Graphene. *Polym. Polym. Compos.* **2008**, *16*, 101–113. [CrossRef]
38. Shinde, S.K.; Dubal, D.P.; Ghodake, G.S.; Gomez-Romero, P.; Kim, S.; Fulari, V.J. Influence of Mn incorporation on the supercapacitive properties of hybrid CuO/$Cu(OH)_2$ electrodes. *RSC Adv.* **2015**, *5*, 30478–30484. [CrossRef]
39. Jimenez-Relinque, E.; Grande, M.; Duran, T.; Castillo, Á.; Castellote, M. Environmental impact of nano-functionalized construction materials: Leaching of titanium and nitrates from photocatalytic pavements under outdoor conditions. *Sci. Total Environ.* **2020**, *744*, 140817. [CrossRef]

40. The European Chemicals Agency. Available online: https://echa.europa.eu/registration-dossier/-/registered-dossier/15560/6/2/1 (accessed on 14 September 2022).
41. Bathla, A.; Younis, S.A.; Pal, B.; Kim, K.H. Recent progress in bimetallic nanostructure impregnated metal-organic framework for photodegradation of organic pollutants. *Appl. Mater. Today* **2021**, *24*, 101105. [CrossRef]
42. Bathla, A.; Lee, J.; Younis, S.A.; Kim, K.H. Recent advances in photocatalytic reduction of CO_2 by TiO_2– and MOF–based nanocomposites impregnated with metal nanoparticles. *Mater. Today Chem.* **2022**, *24*, 100870. [CrossRef]
43. Ouyang, T.; Wang, H.J.; Huang, H.H.; Wang, J.W.; Guo, S.; Liu, W.J.; Zhong, D.C.; Lu, T.B. Dinuclear Metal Synergistic Catalysis Boosts Photochemical CO_2-to-CO Conversion. *Angew. Chem. Int. Ed.* **2018**, *57*, 16480–16485. [CrossRef]
44. Guo, Z.; Cheng, S.; Cometto, C.; Anxolabéhère-Mallart, E.; Ng, S.M.; Ko, C.C.; Liu, G.; Chen, L.; Robert, M.; Lau, T.C. Highly Efficient and Selective Photocatalytic CO_2 Reduction by Iron and Cobalt Quaterpyridine Complexes. *J. Am. Chem. Soc.* **2016**, *138*, 9413–9416. [CrossRef]
45. Tamaki, Y.; Koike, K.; Ishitani, O. Highly efficient, selective, and durable photocatalytic system for CO_2 reduction to formic acid. *Chem. Sci.* **2015**, *6*, 7213–7221. [CrossRef]